

Characteristics of Thermo Diffusion and Buoyant Force Effects in MHD Flow of Copper and Titanium Dioxide Nanoparticles Suspended in Water between Infinite Vertical Plates

Shaik Nazia¹, B Seshaiah²

¹Research Scholar, Department of Mathematics, Jawaharlal Nehru Technological University Anantapur, Ananthapuramu-515002, Andhra Pradesh, India, shaiknazia636@gmail.com ²Department of Basic Sciences (Mathematics), Santhiram Engineering College, Nandyal-518501, Affiliated to Jawaharlal Nehru Technological University Anantapur, Ananthapuramu, India, Seshu.maths@gmail.com

This study explores the heat and mass transfer characteristics of an inconsistent, MHD condensed nanoliquid flow over a stretched sheet under a transverse magnetic field and thermal impacts. The theoretical framework examines two types of nanofluids, Ag-water-based and TiO2- water -based. By converting the governing differential equations into nonlinear ODE's and subsequently employing a standard perturbation approach with appropriate boundary conditions, the solutions are obtained for various physical parameters. The graphical representation and comprehensive analysis of the consequences of these characteristics on dimensionless momentum, energy, and concentration outlines are presented. Comparisons with existing literature demonstrate favourable agreement. Tabulated numerical implications of material abundances, such as the local skin conflict, the local Nusselt numeral, and the local Sherwood numeral, are also furnished. The study reveals that increasing thermal radiation reduces velocity and temperature while enhanced chemical process efficiency decreases concentration levels. Moreover, an increased Soret parameter results in higher velocity and concentration measurements. Notably, TiO2 nanofluids exhibit significantly higher velocities compared to Ag nanofluids when based on water.

Keywords: Nano fluid, heat source parameter, permeable object, thermal diffusion.

1. Introduction

Nanofluids are advanced colloidal suspensions of nanoparticles—such as metals, metal oxides, or carbon-based materials like graphene—dispersed in base fluids like water, ethylene glycol, or oil. Due to the nanoparticles' high surface area and thermal conductivity,

nanofluids exhibit superior thermal properties, significantly enhancing the heat transfer capabilities of traditional fluids. This has led to their widespread application across industries. In automotive and aerospace engineering, nanofluids serve as efficient coolants for engines and heat exchangers, improving system performance and durability. In electronics, they aid in thermal management by dissipating heat in high-performance devices such as CPUs and lasers, preventing overheating. Nanofluids also improve the efficiency of solar collectors in renewable energy by enhancing heat absorption and transfer. In biomedicine, they facilitate targeted drug delivery, thermal therapies, and improved imaging, while in environmental and chemical engineering, they enhance pollutant removal and reaction rates. With their remarkable ability to optimize heat transfer, nanofluids represent a transformative advancement in fluid technology, impacting numerous scientific and industrial applications. The concept of enhancing fluid thermal capabilities by dispersing nanometer-sized particles into a hosting fluid was initially proposed by Masuda et al. [1] in 1993 and further developed by Choi [2] in 1995. This idea led to the creation of nanofluids, wherein fluids with nanoparticle mixtures exhibit approximately 40% greater thermal conductivity compared to corresponding fluids without nanoparticles, according to Eastman et al [3]. Raghunath et al. [4] have studied the effects of thermodynamic and buoyancy forces on Cu and TiO₂ nanoparticles in engine oil flow over an inclined permeable surface, highlighting the improved heat transfer capabilities in such systems. Similarly, Dandu et al. [5] investigated the impact of thermal radiation and chemical reactions on the flow of Casson hybrid nanofluids through porous media, emphasizing the influence of thermophoresis and Brownian motion. The role of Hall current and thermal radiation in 3D rotating hybrid nanofluid flows was examined by Kodi et al. [6], who demonstrated the benefits of internal heat absorption in enhancing thermal efficiency. Additionally, Raju et al. [7] explored the chemical radiation and Soret effects in the unsteady MHD flow of Jeffrey nanofluids over inclined surfaces, providing insights into their potential for industrial applications. Vaddemani et al. [8] focused on the combined effects of Hall current, activation energy, and diffusion-thermo on MHD Casson nanofluids, showing how Brownian motion and thermophoresis enhance heat and mass transfer in porous media. Raghunath [9] further analyzed heat and mass transfer in unsteady MHD nanofluid flows over vertical porous plates, accounting for chemical reactions, radiation, and Soret effects. Lastly, Kodi et al. [10] studied the influence of diffusion thermo and chemical reactions on Jeffrey nanofluids, specifically in MHD flows over inclined surfaces with radiation absorption. Furthermore, Shaw et al. [11] scrutinized the microrevolving of Casson-Carreau nanomaterials within MHD, incorporating sliding effects computationally. Sastry et al. [12] expresseddiscussed the dynamic 3D micropolar nanoliquid stream through a constricting channel, pertinent to cardiovascular health. Nayak et al. [13] investigated glide speed, thermal radiation, and magnetohydrodynamic effects in the vicinity of the stagnation point stream along an extending surface.

Thermal radiation, the emission of electromagnetic waves due to the thermal motion of particles within matter, plays a crucial role in various scientific and engineering applications. In fluid dynamics, thermal radiation significantly impacts the heat transfer processes in complex flow systems, especially when combined with factors like magnetic fields, chemical reactions, and nanofluids. For instance, Yadav et al. [14] examined the effects of temperature-dependent thermal conductivity and viscosity on the convection of Jeffrey fluid

in rotating porous media, showing how thermal radiation can enhance heat transfer. Zhang et al. [15] explored mixed convection in a Darcy-Forchheimer Maxwell fluid and highlighted the effects of radiation absorption and diffusion, demonstrating its importance in energy systems. Yadav et al. [16] further analyzed the role of rotation and thermal conductivity variations in the convection of Casson fluid, emphasizing how radiation can influence cellular convective movement. In MHD flows, Yedhiri et al. [17] investigated the effects of Joule heating, Hall current, and radiation absorption, showing the thermal management benefits of radiative heat transfer. Kommaddi et al. [18] studied Jeffrey fluid under rotating conditions, highlighting how radiation absorption improves heat and mass transfer in chemically reacting flows. Additional studies by Kodi et al. [19] on Jeffrey nanofluid flows with Cu and TiO₂ nanoparticles, and Reddy et al. [20] on porous media flows with radiation and Soret effects, further illustrate the broad applications of thermal radiation. Lastly, Raghunath and colleagues [21-23] emphasized the influence of radiation absorption and magnetic fields on MHD Casson fluid flows in porous media, demonstrating its relevance in optimizing heat transfer in engineering and environmental applications. Together, these studies underscore the versatility of thermal radiation in enhancing heat transfer and energy efficiency across various scientific and industrial applications.

Magnetohydrodynamics (MHD) with heat transfer in the presence of radiation and diffusion has attracted considerable interest from researchers due to its broad applications across fields such as astrophysics, geophysics, and engineering. In astrophysics and geophysics, MHD is used to study stellar and solar structures, radio wave propagation through the ionosphere, and other phenomena where electrically conducting fluids interact with electromagnetic fields. When a conducting fluid flows through a magnetic field, it generates an electric field and, consequently, an electric current. This current interacts with the magnetic field, producing a body force that affects fluid motion. These interactions are naturally present and are utilized in engineered devices, including MHD propulsion systems, power generators, electron beam systems, traveling wave tubes, and MHD pumps and bearings.

Several studies have advanced our understanding of MHD in nanofluid flows with heat transfer and diffusion effects. Kuznetsov and Nield [24] examined nanofluid flow through natural convection along a vertical boundary. Hamad and Pop [25] studied unsteady hydromagnetic nanofluid flow along a porous flat plate with uniform heat generation in a rotating frame. Further, Hamad et al. [26] analyzed the effect of a uniform magnetic field on nanofluid convection along a semi-infinite vertical plate, focusing on the conductive nanofluid boundary layer flow of a pure liquid with nanoparticles under magnetic induction, heat sources, and injection effects. Chamkha and Aly [27] developed a model incorporating Brownian motion and thermophoresis in nanofluid flow. Turkyilmazoglu and Pop [28] investigated heat and mass flow over a radiating conductive nanofluid along a vertical plate, while Turkyilmazoglu [29] addressed heat and mass flow in magnetic nanofluid slip flow with a fixed magnetic field relative to the fluid or plate. Rushi Kumar et al. [30] explored the influence of thermal diffusion and radiation on unsteady free convection flow, further contributing to the understanding of MHD nanofluid dynamics in complex thermal environments.

This analysis specifically focuses on comparing the thermo conductive of TiO2 and Cu microparticles when dispersed in machine lubricant (EO), considering their significant

applications in electronic contraptions, energy partitions, cooling approaches, warmth pumps, and warmth exchangers. TiO2, recognized for its non-toxicity, affordability, and stability, demonstrates moderately heightened thermo conductive values (4.00–11.80 W m– 1.0 K-1.0). Leang et al. [31] explored the thermo manners and warmth conception effects of a copper-titanium (Cu-TiO2) mixed nanoliquid, comparing it with the belongings of established Cu and TiO2 nanoliquids. Ali et al. [32] suggested a Brinkman classification liquid instance to scrutinize the constitution consequences of nanoliquids utilizing machine lubricant and kerosene lubricant with MoS2 microparticles on a revolving consistency. Vashaghani et al. [33] determined the consistency and warmth transfer speed of TiO2 machine lubricant nanofluids using the superheated wire strategy and verified their consequences with empirical data. Khat et al. [34] recently assessed the thermo implementation of moisture and machine lubricant nanoliquids under miscellaneous geometrical configurations, believing grooved consistencies in warmth exchangers with dissimilar Reynolds numerals for moisture and machine lubricant, based on experimental data. Rajo et al. [35] provided a proximate examination of the thermo behavior of machine lubricant (EO) microparticles, integrating unstable magnetic specialization and thermo radiation impacts in a penetrable channeler. Rayindranath et al. [36] researched the behavior of Casson nanofluid in MHD convective movement around a semi-boundless predisposed penetrable movable leaf considering warmth and energy transfer.

Building upon the findings from Ravindra and Ramakrishna [36], we extended their investigation to explore the consequences of thermal disbandment and thermophysical properties on free convective warmth and energy transmission, along an upright plate immersed in a penetrable object subjected to radiation and persistent warmth inception underneath inconsistent frontier conditions. Both Ag- water and TiO2- water nanofluids were theoretically analyzed. The PDE's were solved analytically utilizing the regular perturbation strategy. The study examines the influence of relevant flow characteristics on speed, energy, and mass transport, including skin variance, thermal conductivity, and rate of mass transmission. The results are presented utilizing graphical and tabular formats.

2. Mathematical Representation of the current phenomena

The channel considers unstable MHD bi-dimensional movement of a laminar, thick, impenetrable, electrically manipulating liquid beyond a semi-boundless upright absorptive moving plating entrenched in an invariant penetrable object, subjected to an invariant transverse magnetic specialisation, thermo radiation, and homogeneous chemical response. The y*-axis is abrupt to the upward movement of the gush. A consistent exterior magnetic field B0 acts along the y tendency, with negligible influenced magnetic specialization and exterior electric domain due to control polarization.

- The magnetic field applied transversely and the magnetic Reynolds numeral are considered very tiny, making the influenced magnetic specialization and Hall impact insignificant.
- The liquid is a water -based nanoliquid possessing nanoparticles of silver (Ag) and titanium oxide (TiO2).
- Fluid properties, excluding the density variation with temperature, are presumed to *Nanotechnology Perceptions Vol. 20 No.6 (2024)*

remain constant.

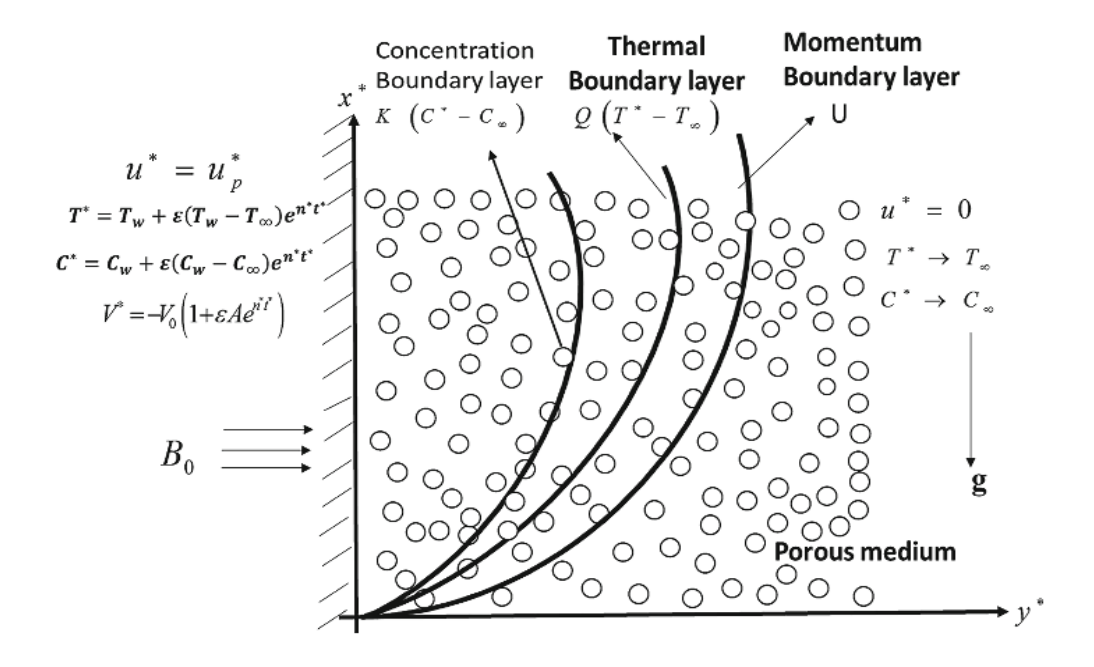


Figure: 1depicts the physical structure of the problem.

- The concentration of the diffusing species is minimal compared to other chemical species; therefore, the Soret and Dufour impacts are ignored, with the concentration far from the wall $(C\infty)$ being extremely small.
- Due to the semi-boundless plane consistency hypothesis, the gush variables hinge only on y* and time t*.
- A chemical reaction occurs within the flow, and all thermophysical properties are considered constant in the linear momentum equation, applying the Boussinesq approximation.

$$\frac{\partial v^*}{\partial y^*} = 0$$

$$\frac{\partial u^*}{\partial t^*} + v^* \frac{\partial u^*}{\partial y^*} = -\frac{\mu_{nf}}{\rho_{nf}} \frac{\partial^2 u^*}{\partial y^{*2}} + \frac{(g\beta_T)_{nf}}{\rho_{nf}} (T^* - T_\infty^*) + \frac{(g\beta_C)_{nf}}{\rho_{nf}} (C^* - C_\infty^*) - \frac{\sigma B_0^2}{\rho_{nf}} u^* - \frac{\mu_{nf}}{\rho_{nf}} \frac{u^*}{k^*} \tag{2}$$

1553 Shaik Nazia et al. Characteristics of Thermo Diffusion and....

$$\left(\frac{\partial T^*}{\partial t^*} + v^* \frac{\partial T^*}{\partial y^*}\right) = \alpha_{nf} \frac{K}{\left(\rho C_p\right)_{nf}} \frac{\partial^2 T^*}{\partial y^{*2}} - \frac{1}{\left(\rho C_p\right)_{nf}} \frac{\partial q_r^*}{\partial y^*} + \frac{Q^*}{\left(\rho C_p\right)_{nf}} (T^* - T_{\infty}^*) \tag{3}$$

$$\frac{\partial C^*}{\partial t^*} + v^* \frac{\partial C^*}{\partial y^*} = D \frac{\partial^2 C^*}{\partial y^{*2}} - K^* (C^* - C_{\infty}^*) + D_1 \frac{\partial^2 T^*}{\partial y^{*2}}$$

$$\tag{4}$$

Taking into account the aforementioned hypotheses, the fitting limit requirements for the disbandments of momentum, energy, and concentration are as observes:

$$t^{*} < 0, \quad C^{*} = C_{\infty}^{*}, \quad u^{*}(y^{*}, t^{*}) = 0, \quad T^{*} = T_{\infty}^{*}$$

$$t^{*} \ge 0, \quad C^{*} = C_{w}^{*} + \varepsilon (C_{w}^{*} - C_{\infty}^{*}) e^{in^{*}t^{*}}, \quad T^{*} = T_{w}^{*} + \varepsilon (T_{w}^{*} - T_{\infty}^{*}) e^{in^{*}t^{*}}, \quad u^{*}(y^{*}, t^{*}) = u_{0} \quad \text{at} \quad y^{*} = 0$$

$$T^{*} \to T_{\infty}^{*}, \quad u^{*}(y^{*}, t^{*}) = 0, C^{*} \to C_{\infty}^{*} \qquad \text{as} \quad y^{*} \to \infty$$

$$(5)$$

In the provided equations, u^* and v^* characterize the velocity segments along the x^* and y^* axes, respectively. The thermal expansion coefficient of the nanofluid is indicated by β nf, σ denotes the fluid's electrical conductivity. The density of the nanofluid is denoted by ρ_{nf} , and μ nf refers to its viscosity. The heat capacitance of the nanofluid is represented by $\rho C p_{nf}$, and g stands for gravitational acceleration. The permeability of the porous medium is expressed by K^* , the temperature of the nanofluid by T^* , and the temperature-dependent volumetric heat source rate by Q. Additionally, α_{nf} signifies the thermo diffusivity of the nanoliquid. These parameters are defined as follows [36], with phi representing the nanoparticle solid volume fraction, and K_{nf} and K_s denoting the thermal conductivities of the base fluid and solid, respectively. Table 1 provides the thermophysical properties of water, copper, and titanium used for code validation. These parameters are precisely expressed as per Abbasi [37], [38], and Ahamed et al. [39].

Table 1. Thermo-physical properties (see [37, 38, and 39]).

Tuble 1. Thermo physical properties (see [57, 50, and 55]).					
Materials	$\rho (kg/m^3)$	C _p (J/kgK)	k (W/mK)		
water H2O	997.1	4179	0.613		
Silver (Ag)	8933	1910	0.1440		
Titanium oxide (Ti O2)	4250	686.20	8.9538		

Table 2: Requisite posited correlations of Ag and TiO₂ based- water nanoparticles [37, 38, 39]

Properties	Nanofluid specifications
Density	$\rho_{nf} = (1 - \phi)\rho_f + \phi\rho_s,$
Heat capacity	$\left(\rho C_{p}\right)_{nf} = \left(1 - \phi\right)\left(\rho C_{p}\right)_{f} + \phi\left(\rho C_{p}\right)_{s},$
Thermo heat capacity	$(\rho\beta)_{nf} = (1-\phi)(\rho\beta)_f + \phi(\rho\beta)_s$
Thermal conductivity	$K_{nf} = K_f \left(\frac{K_s + 2K_f - 2\phi(K_f - K_s)}{K_s + 2K_f + 2\phi(K_f - K_s)} \right),$

Absolute viscosity	$\mu_{nf} = \left(\frac{\mu_f}{(1-\phi)^{2.5}}\right),$
Electrical conductivity	$lpha_{nf} = \left(\frac{K_{nf}}{\left(ho C_p\right)_{nf}}\right)$

In this context, the constant $-v_0$ is used to signify the normal velocity at the surface, which is positive for suction $(v_0 > 0)$ and unfavorable for botching injection $(v_0 < 0)$.

We examine a mathematical model proposed by Cramer and Pai [40] for an optically thin gray gas near equilibrium. This model was further discussed by Grief et al. [41].

$$\frac{\partial q_r^*}{\partial y^*} = 4\left(T^* - T_w^*\right)I\tag{7}$$

Where
$$I = \int_{0}^{\infty} K_{\lambda\omega} \left(\frac{\partial_{eb\lambda}}{\partial T} \right)_{\omega} d\lambda$$
, (8)

 $K_{\lambda\omega}$ is the absorption factor at the partition and eb λ is Planck's operation.

To standardize the mathematical representation of the physical scenario, incorporate the ensuing dimensionless quantities.

$$u = \frac{u^{*}}{U_{0}}, v = \frac{v^{*}}{v_{0}}, y = \frac{v_{0}y^{*}}{v_{f}}, t = \frac{t^{*}v_{0}^{2}}{v_{f}}, \theta = \frac{T^{*}-T_{\infty}^{*}}{T_{w}^{*}-T_{\infty}^{*}} \phi = \frac{C^{*}-C_{\infty}^{*}}{C_{w}^{*}-C_{\infty}^{*}}, n = \frac{n^{*}\theta_{f}}{v_{0}^{2}}, S = \frac{v_{0}}{U_{0}}.$$

$$k = \frac{k^{*}v_{0}^{2}}{v_{f}^{2}}, \Pr = \frac{\mu_{f}C_{pf}}{K_{f}}, Sc = \frac{v_{f}}{D_{m}}, M = \frac{\sigma B_{0}^{2}v_{f}}{\rho_{f}v_{0}^{2}}, Q = \frac{Q^{*}v_{f}}{(\rho C_{p})_{f}v_{0}^{2}}, K_{r} = \frac{v_{f}K^{*}}{v_{0}^{2}}, R_{d} = \frac{4I_{1}v_{f}}{(\rho C_{p})_{f}v_{0}^{2}}$$

$$S_{r} = \frac{D_{1}K(T_{w}^{*}-T_{\infty}^{*})}{v_{f}(C_{w}^{*}-C_{\infty}^{*})}, Gr = \frac{v_{f}g(\rho\beta_{T})_{f}(T_{w}^{*}-T_{\infty}^{*})}{U_{0}v_{0}^{2}}, Gm = \frac{v_{f}g(\rho\beta_{c}^{*})_{f}(C_{w}^{*}-C_{\infty}^{*})}{U_{0}v_{0}^{2}}$$

$$(9)$$

The equations (2) to (4) in their non-dimensional form are

$$A\left(\frac{\partial u}{\partial t} - S\frac{\partial u}{\partial y}\right) = D\frac{\partial^2 u}{\partial y^2} + B(Gr\theta + Gm\phi) + u(M+1/k)$$
(10)

$$C\left(\frac{\partial\theta}{\partial t} - S\frac{\partial\theta}{\partial y}\right) = \frac{1}{\Pr}\left(E\frac{\partial^2\theta}{\partial y^2} - (R_d + Q)\theta\right)$$
(11)

$$\frac{\partial \phi}{\partial t} - S \frac{\partial \phi}{\partial y} = \frac{1}{Sc} \frac{\partial^2 \phi}{\partial y^2} + Sr \frac{\partial^2 \phi}{\partial y^2} - Kr\phi \tag{12}$$

Where
$$A = \left((1 - \phi) + \phi \left(\frac{\rho_s}{\rho_f} \right) \right)$$
, $B = \left((1 - \phi) + \phi \left(\frac{(\rho \beta)_s}{(\rho \beta)_f} \right) \right)$, $C = \left((1 - \phi) + \phi \left(\frac{(\rho C_p)_s}{(\rho C_p)_f} \right) \right)$

1555 Shaik Nazia et al. Characteristics of Thermo Diffusion and....

$$D = \left(\frac{1}{(1-\phi)^{2.5}}\right), E = \left(\frac{(1+2\phi)+(2-2\phi)\left(\frac{K_f}{K_s}\right)}{(1-2\phi)+(2+2\phi)\left(\frac{K_f}{K_s}\right)}\right)$$

The related boundary conditions are defined as follows

$$t^* < 0, \quad \theta = 0, \quad u = 0, \quad \phi = 0$$

 $t^* \ge 0, \quad u = 1, \quad \theta = 1 + \varepsilon e^{int}, \quad \phi = 1 + \varepsilon e^{int} \quad \text{at } y = 0$
 $u = 0, \quad \theta \to 0, \quad \phi \to 0 \quad \text{as } y \to \infty$

$$(13)$$

3. Method of Solution

Equations (10) through (12) are partial differential equations lacking a solution in closed form. Nonetheless, one can solve them by converting them into a series of ODE's via the perturbation strategy. Consequently, portray the distributions of momentum, energy, and concentration using both harmonic and non-harmonic processes in the subsequent manner.

$$u(y,t) = u_0(y) + \varepsilon u_1(y)e^{nt} + O(\varepsilon^2)$$

$$\theta(y,t) = \theta_0(y) + \varepsilon \theta_1(y)e^{nt} + O(\varepsilon^2)$$

$$\phi(y,t) = \phi_0(y) + \varepsilon \phi_1(y)e^{nt} + O(\varepsilon^2)$$
(14)

By inserting Equations (14) into Equations (10) through (12), matching the harmonic and non-harmonic components, and disregarding more elevated level components of ε , we can derive the subsequent sets of equations at both zeroth and first orders.

$$Du_0'' + ASu_0' - \left(M + \frac{1}{k}\right)u_0 = B\left(-Gr\theta_0 - Gm\phi_0\right) - \left(M + \frac{1}{k}\right)$$
(15)

$$E\theta_0'' + \Pr CS\theta_0 - (R_d + Q)\Pr \theta_0 = 0$$
(16)

$$\varphi_0^{ll} + SS_c \varphi_0^l - \operatorname{Sc} \operatorname{Kr} \varphi_0 = -\operatorname{Sc} \operatorname{Sr} \theta_0^{ll}$$
(17)

$$Du_1'' + ASu_1' - ((M+1/k) + An)u_1 = B(-Gr \theta_1 - Gm \phi_1) - u_0' - (M + \frac{1}{k})$$
(18)

$$E\theta_1'' + \Pr CS\theta_1' - (n+Q)\Pr \theta_1 = -\Pr \theta_0'$$
(19)

$$\varphi_1^{ll} + SS_c \varphi_1^l - \operatorname{Sc}(Kr + n) \varphi_1 = -\operatorname{Sc} \varphi_0^l - \operatorname{Sc} \operatorname{Sr} \theta_1^{ll}$$
(20)

The associated boundary conditions are

$$u_0 = 1, \ \theta_0 = 1, \ u_1 = 0, \ \phi_1 = 1 \ \theta_1 = 1, \ \phi_0 = 1, \ at \quad y = 0$$

 $u_0 \to 0, \ \theta_0 \to 0, \ u_1 \to 0, \ \phi_1 \to 0, \ \theta_1 \to 0, \ \phi_0 \to 0 \ as \quad y \to \infty$
(21)

The solutions obtained from solving equations (15) through (20) with the boundary conditions (21) are as follows.

$$\varphi_0 = A_4 \exp(-m_3 y) + A_3 \exp(-m_1 y) \tag{22}$$

$$\theta_0 = \exp(-m_1 y) \tag{23}$$

$$u_0 = 1 + A_{10} \exp(-m_3 y) + A_9 \exp(-m_5 y) + A_{11} \exp(-m_5 y)$$
(24)

$$\varphi_1 = A_7 \exp(-m_3 y) + A_5 \exp(-m_1 y) + A_8 \exp(-m_4 y) + A_6 \exp(-m_2 y)$$
 (25)

$$\theta_1 = A_1 \exp(-m_1 y) + A_2 \exp(-m_2 y)$$
 (26)

$$u_1 = 1 + A_{17} \exp(-m_6 y) + A_{12} \exp(-m_1 y) + A_{14} \exp(-m_3 y) +$$

$$A_{15} \exp(-m_4 y) + A_{13} \exp(-m_2 y) + A_{16} \exp(-m_5 y) + A_{17} \exp(-m_6 y)$$
 (27)

By solving equations (15) through (20) with the given boundary conditions (21), we can derive the velocity, temperature, and concentration profiles within the boundary layer

$$u = 1 + b_{11} \exp(-m_5 y) + b_{10} \exp(-m_3 y) + b_9 \exp(-m_1 y) + \varepsilon e^{int} \begin{bmatrix} (1 + b_{14} \exp(-m_3 y) + b_{17} \exp(-m_6 y) + b_{18} \exp(-m_6 y) + b_{18} \exp(-m_1 y) + b_{18} \exp(-m_2 y) + b_{18} \exp(-m_2 y) + b_{18} \exp(-m_2 y) \end{bmatrix}$$
(28)

$$\theta = b_4 \exp(-m_3 y) + b_3 \exp(-m_1 y) + \varepsilon e^{int} \begin{bmatrix} b_6 \exp(-m_2 y) + b_8 \exp(-m_4 y) + b_8 \exp(-m_4 y) + b_9 \exp(-m_3 y) \\ b_5 \exp(-m_1 y) + b_7 \exp(-m_3 y) \end{bmatrix}$$
(29)

$$\phi = \exp(-m_1 y) + \varepsilon e^{\inf} [b_2 \exp(-m_2 y) + b_1 \exp(-m_1 y)]$$
(30)

A crucial physical factor at the boundary involves skin friction and the Nusselt number, typically expressed in non-dimensional form and derived from it.

$$\tau = \left(\frac{\partial u}{\partial y}\right)_{y=0} = -(m_1b_9 + m_3b_{10} + m_5b_{11}) - \varepsilon e^{nt}(m_1b_{12} + m_2b_{13} + m_3b_{14} + m_4b_{15} + m_5b_{16} + m_6b_{17})$$
(31)

$$Nu = -\left(\frac{\partial \theta}{\partial y}\right)_{y=0} = m_1 b_3 + m_3 b_4 + \varepsilon e^{int} (m_1 b_5 + m_2 b_6 + m_3 b_7 + m_4 b_8)$$
 (32)

4. Discussion of the Results

To gain material insights into the concern, we conducted arthematical computations for dimensionless momentum, energy, and species concentration, as well as for skin variance and Nusselt numeral, using specific parameter values for two distinct water -based nanofluids. We presented dual resolutions for TiO2- water and Ag-water nanofluids, depicted in Figs. 2-12. Tableland 1 provides the thermophysical possessions of water and the microelements (Ag and TiO2). To validate our findings, we compared the skin conflict factor

and local Nusselt numeral with those of Ravindra and Ramakrishna [36] across various conditions, as shown in Table 4. The comparison exemplifies outstanding consensus, affirming the exactness of our developments.

4.1 Impact of magnetic field parameter (M):

Fig. 2 displays nanofluid velocity profiles across varying magnetic field (M) for Ag- water and TiO2- water nanoparticles. The velocity of the nanofluid diminishes as the magnetic field strength enlarges, indicating the influence of a transverse magnetic domain known as the Lorentz strength, which resists liquid movement in the perimeter layer. These findings align with expectations, as magnetic fields impede natural convection flow. Additionally, the nanoliquid momentum is more downward for the base liquid compared to TiO2 nanoparticles, which exhibit the highest velocity peak among Ag nanoparticles.

4.2 Impact of suction parameter (S):

In Fig. 3, the impact of the suction factor (S) on fluid velocity is depicted. The results indicate that improving the suction factor (S) directs to a lowering in fluid velocity across the boundary layer, both for regular fluid and nanofluids containing Ag-water and TiO2- water nanoparticles. Importantly, it is noted that the effect of the suction factor (S) on liquid velocity is more pronounced for nanoliquids with Ag and TiO2 microparticles. Additionally, it is obeyed that the highest momentum of Ag- water nanofluid surpasses that of TiO2- water nanofluid around y=1.

4.3 Impact of Thermal and Mass Grashof number:

The consequence of the thermal Grashof numeral (Gr) and mass Grashof numeral (Gm) on the momentum diffusion for Ag- water and TiO2- water nanofluids are shown in Figs. 4 and 5 respectively. The Grashof numbers, both thermal (Gr) and mass (Gm), are dimensionless parameters that quantify the relative significance of buoyancy forces in a fluid. The thermal Grashof number (Gr) pertains to buoyancy forces induced by temperature gradients, while the mass Grashof number (Gm) relates to buoyancy forces arising from concentration gradients. For both Ag-water and TiO2- water nanofluids, an increase in either Gr or Gm results in an enhanced velocity distribution. This enhancement occurs because higher Gr values indicate stronger thermal buoyancy forces, which promote more vigorous convection and fluid movement. Similarly, higher Gm values indicate stronger mass buoyancy effects due to concentration differences, further stimulating fluid motion. Consequently, as Gr and Gm values increase, the buoyancy-driven forces become more dominant compared to viscous forces, leading to an overall enhances in the velocity of the nanoliquids. This behavior underscores the effectiveness of nanofluids in enhancing heat and mass transfer due to their improved responsiveness to thermal and concentration gradients compared to conventional fluids.

4.4 Impact of thermal radiation (Rd):

Figs. 6 and 7 show the consequences of thermal radiation on the velocity and temperature disbandment of AG- water and TiO2- water nanofluids, respectively. As the thermal radiation factor enlarges, momentum and temperature lower due to enhanced heat emission from the fluids. As the thermal radiation factor enlarges, more heat is emitted from the nanofluids due to enhanced radiation. This diminishes velocity and temperature as the liquid

loses thermal energy more rapidly, impacting the buoyant forces driving fluid motion and overall fluid temperature.

4.5 Impact of thermal radiation (Rd):

Figs. 6 and 7 show the consequences of thermal radiation on the velocity and temperature disbandment of AG- water and TiO2- water nanofluids, respectively. As the thermal radiation factor enlarges, momentum and temperature lower due to enhanced heat emission from the fluids. As the thermal radiation factor enlarges, more heat is emitted from the nanofluids due to enhanced radiation. This diminishes velocity and temperature as the liquid loses thermal energy more rapidly, impacting the buoyant forces driving fluid motion and overall fluid temperature.

4.6 Impact of thermal diffusion (Sr):

The impact of thermal diffusion on velocity and concentration distribution for Ag- water and TiO2- water nanofluids is illustrated in Figs. 8 and 9, respectively. As the thermal diffusion parameter increases, both velocity and concentration increase in Ag- water and TiO2- water nanofluids. This implies that higher levels of thermal diffusion lead to enhanced fluid movement and greater concentration of the respective nanofluids.

4.7 Impact of Schmidt number (Sc)

Figure 10 illustrates the interpretation in the concentration limit layer of the movement pastureland for H₂, H₂O moisture, and NH₃. This figurine portrays the concentration disbandment within the flow field. Comparing the curves, it is obvious that an increasing Schmidt numeral diminishes the concentration limit layer consistency in all matters. This reduction in the concentration limit layer consistency diminishes the concentration buoyant outcomes, declining liquid outpour. Consequently, the concentration silhouettes decrease along with the concentration boundary layer thickness.

4.8 Impact of Chemical Reaction (Kr)

Figure 11 shows the concentration silhouettes for distinct significances of the destructive chemical reaction parameter (Kr). An enlargement in the chemical response factor suppresses the liquid's concentration. More heightened significances of (Kr) correspond to a decrease in chemical molecular diffusivity, resulting in less diffusion and reduced species transfer. Consequently, an enlargement in Kr will diminish species concentration. The concentration disbandment diminishes at all moments in the movement area as the retort factor grows.

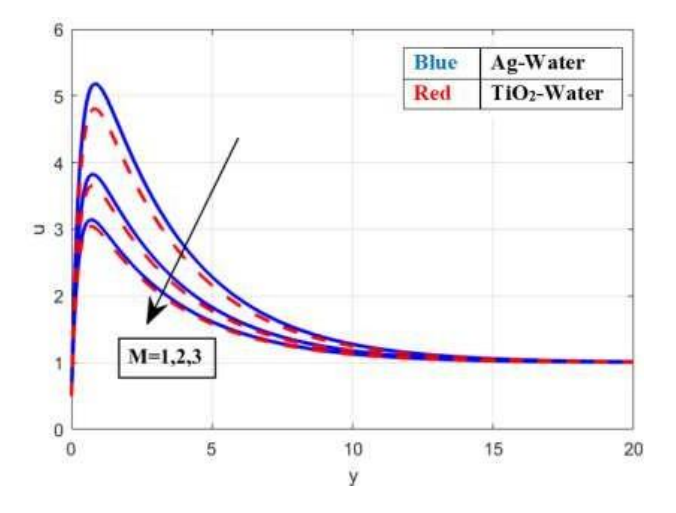


Figure 2: Velocity profiles for Magnetic field parameter

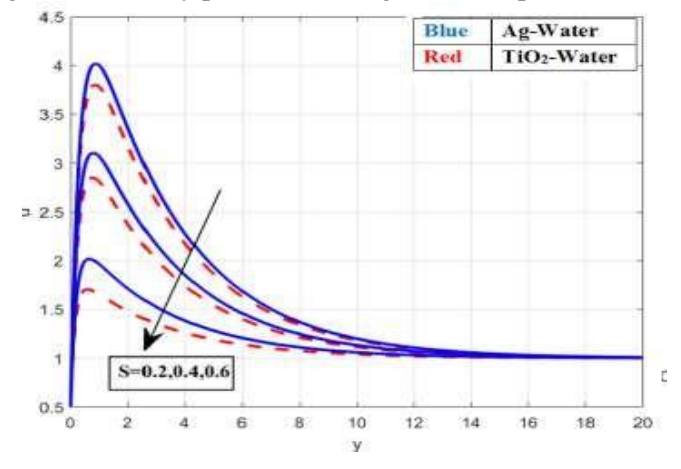


Figure 3: Velocity profiles for Suction parameter

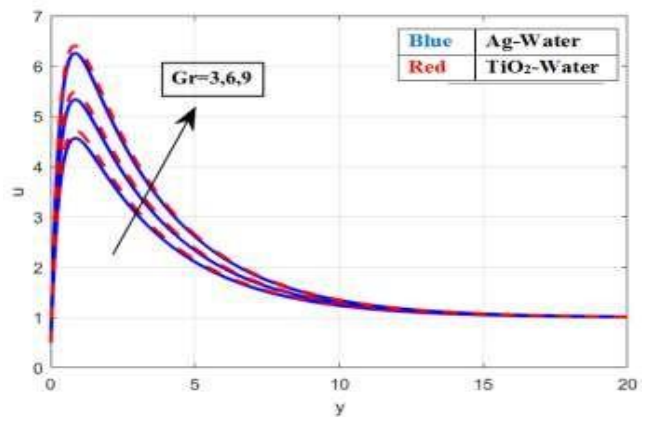


Figure 4: Velocity profiles for Thermal Grashof Number

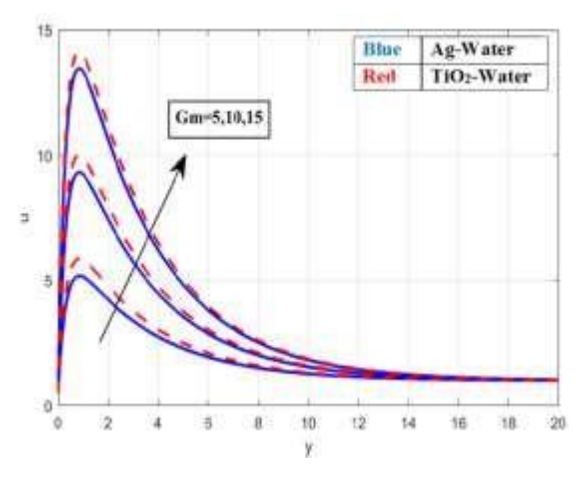


Figure 5: Velocity profiles for Mass Grashof Number

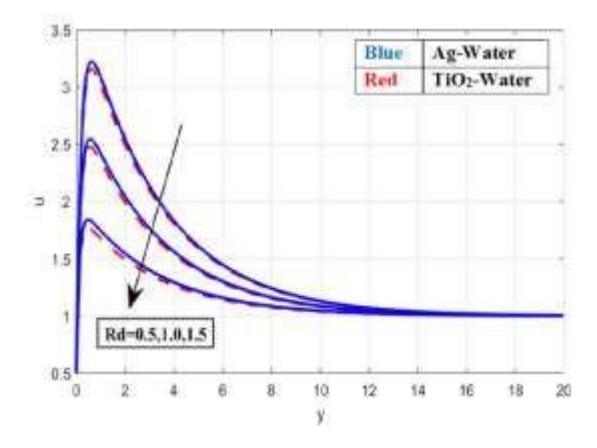


Figure 6: Velocity profiles for thermal radiation

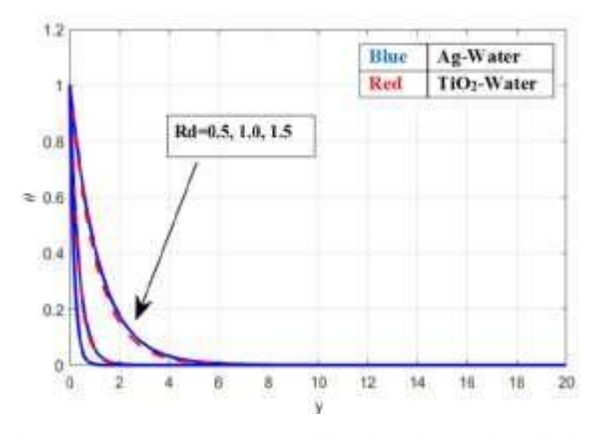


Figure 7: Temperature profiles for thermal radiation

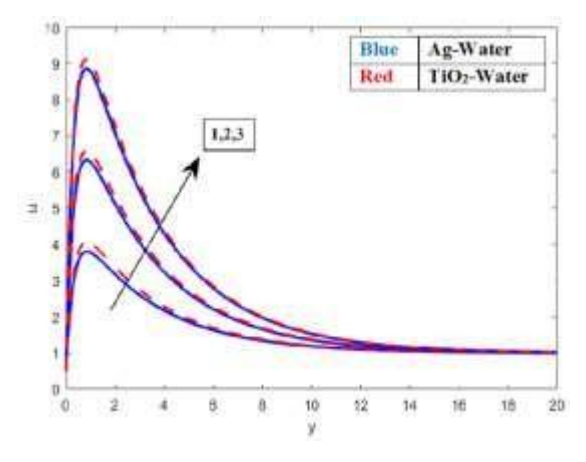


Figure 8: Velocity profiles for thermal diffusion parameter

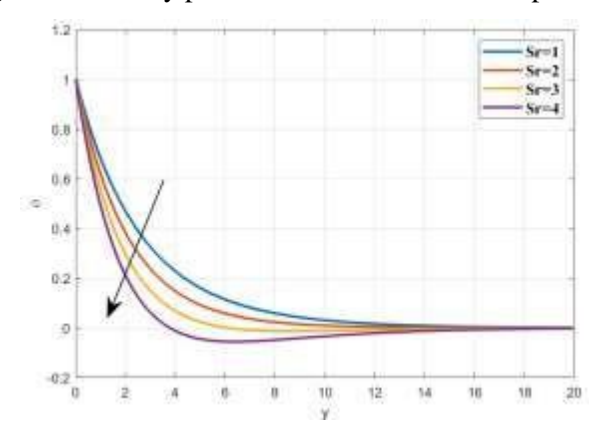


Figure 9: Concentration profiles for thermal diffusion parameter

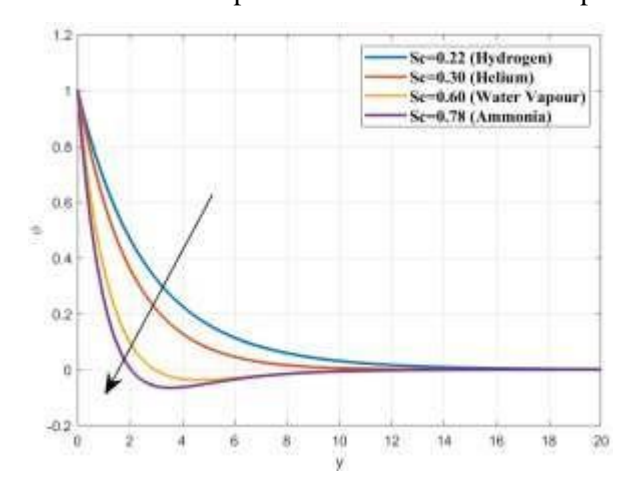


Figure 10: Concentration profiles for Schmidt number

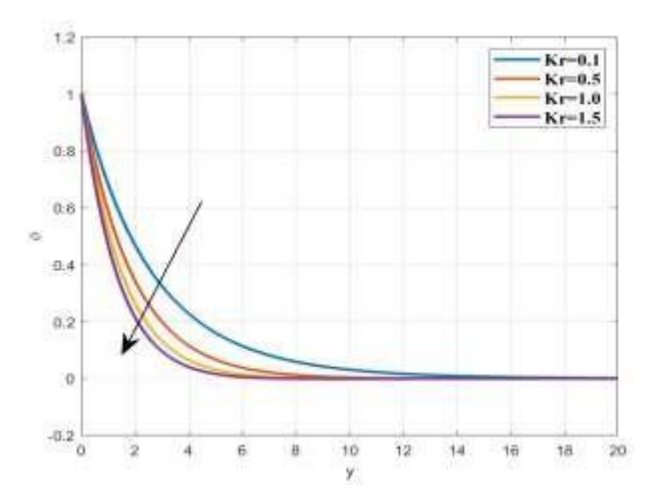


Figure 11: Concentration profiles for Chemical reaction

Table: 3 the consequence of numerous quantities on the skin friction for Sc=0.600, Pr=6.5, Gr=5.0, k=0.50, Kr=0.10, M=1.0, Q=2.0, E=0.010, A=0.50, R=0.10, Gm=3.0, t=0.50, n=1.0, Sr=1.50.

Gr	M	K	Sr	R_d	Kr	Gm	Q	Skin Friction	Skin	Skin Friction	Skin Friction
								for Ag-water	Friction for	for Cu-Water	for TiO2- Water
								fluid Present	TiO ₂ - water	Ravindra and	Ravindra and
								values	fluid Present	Ramakrishna	Ramakrishna
									values	[36] values	[36] values
3	0.5	2	1.5	1	0.5	3	0.5	0.1175	0.3012	0.1175	0.3012
6	0.5	2	1.5	1	0.5	3	0.5	1.9225	1.5165	1.9225	1.5165
9	0.5	2	1.5	1	0.5	3	0.5	3.9568	3.3045	3.9568	3.3045
5	1	2	1.5	1	0.5	3	0.5	4.2675	4.2387	4.2675	4.2387
5	2	2	1.5	1	0.5	3	0.5	1.9475	1.5197	1.9475	1.5197
5	3	2	1.5	1	0.5	3	0.5	0.4625	0.0446	0.4625	0.0446
5	0.5	3	1.5	1	0.5	3	0.5	1.9212	1.5151	1.9212	1.5151
5	0.5	4	1.5	1	0.5	3	0.5	3.0112	2.6845	3.0112	2.6845
5	0.5	6	1.5	1	0.5	3	0.5	3.5752	3.3652	3.5752	3.3652
5	0.5	2	1	1	0.5	3	0.5	0.7550	0.4525	0.7550	0.4525
5	0.5	2	3	1	0.5	3	0.5	5.4653	4.6878	5.4653	4.6878
5	0.5	2	5	1	0.5	3	0.5	10.2652	8.9598	10.2652	8.9598
5	0.5	2	1.5	1	0.5	3	0.5	1.4775	1.1885	1.4775	1.1885
5	0.5	2	15	0.2	0.5	3	0.5	1.5852	1.2446	1.5852	1.2446
5	0.5	2	1.5	0.3	0.5	3	0.5	1.7152	1.3152	1.7152	1.3152
5	0.5	2	1.5	1	1	3	0.5	0.0361	0.2445	0.0361	0.2445
5	0.5	2	1.5	1	5	3	0.5	2.0575	2.1352	2.0575	2.1352
5	0.5	2	1.5	1	10	3	0.5	2.2295	2.2678	2.2295	2.2678
5	0.5	2	1.5	1	0.5	2	0.5	0.9856	0.9882	0.9856	0.9882
5	0.5	2	1.5	1	0.5	4	0.5	1.9352	1.4124	1.9352	1.4124
5	0.5	2	1.5	1	0.5	6	0.5	2.8245	2.1845	2.8245	2.1845

Table: 4 the consequence of numerous quantities on the Nusselt number for Pr=6450, Q=0.50, R_d =1.0, t=0.50.

R_d	Q	Gr	Gm	Nusselt number for Ag- water fluid	Nusselt number for TiO ₂ - water fluid Present
				Present values	values
1	0.5	5	3	0.4565	0.5525
2	0.5	5	3	0.8995	0.6145
3	0.5	5	3	2.2395	1.7825
1	3	5	3	0.9412	1.4645

1	4	5	3	1.4956	1.9454
1	5	5	3	2.4132	2.3751
1	0.5	3	3	0.9874	0.9956
1	0.5	6	3	0.8745	0.8455
1	0.5	9	3	0.7264	0.7447
1	0.5	5	2	0.9956	0.9439
1	0.5	5	4	0.8456	0.8453
1	0.5	5	6	0.7378	0.8120

5. Conclusion

To make the examination more gorgeous, we contemplated two distinguishable kinds of nanoliquids, namely, TiO2-Water and Ag- Water. The determinations are as obeys:

- Fluid velocity diminishes with improving magnetic domain and scution factor significances for both Ag and TiO₂ nanoparticles. Conversely, liquid momentum improves with more elevated significances of the thermal Grashof numeral, mass Grashof numeral, and thermo diffusion factor.
- An increase in the thermal radiation parameter results in a reduction of both velocity and temperature within the fluid. This means that as thermal radiation becomes more significant, the fluid's motion slows down and the overall temperature decreases.
- An increase in the thermal diffusion parameter leads to an increase in both velocity and concentration within the fluid. This indicates that higher thermal diffusion enhances fluid movement and raises concentration levels.
- The concentration decreases with increasing Schmidt number and chemical reaction. This suggests that higher Schmidt numbers and stronger chemical reactions result in lower concentration levels within the fluid.
- The skin friction coefficient is significantly influenced by both the magnetic field and thermal diffusion. This indicates that changes in magnetic field strength and thermal diffusion have a notable impact on the skin friction coefficient within the flow.

References

- 1. Masuda, H., Ebata, A., Teramae, K., Hishinuma, N., (1993). Alteration of thermal conductivity and viscosity of liquid by dispersing ultrafine particles Netsu Bussei 4 227–33
- 2. Choi, U. S., Eastman, J. A., (1995). Enhancing Thermal Conductivity of Fluids with Nanoparticles, 95, 1135.
- 3. Eastman, J. A., Choi, U. S., Li, S., Yu. W., Thompson, L. G., (2001). Anomalously increased effective thermal conductivities of ethylene glycolbased nanofluids containing copper nanoparticles, Appl. Phys. Lett, 78, 718-128.
- 4. Kodi, R., Vaddemani, R. R., Kommaddi, H., Noeiaghdam, S., & Fernandez-Gamiz, U. (2024). Thermodynamic and buoyancy force effects of Cu and TiO2 nanoparticles in engine oil flow over an inclined permeable surface. Journal of King Saud University Science, 36(10), Article 103434. https://doi.org/10.1016/j.jksus.2024.103434.
- 5. Dandu, S., Chitrapu, V. R. M., & Kodi, R. (2024). An investigation into the impact of thermal radiation and chemical reactions on the flow through porous media of a Casson

- hybrid nanofluid including unstable mixed convection with stretched sheet in the presence of thermophoresis and Brownian motion. Open Physics, 22(1), Article 20240043. https://doi.org/10.1515/phys-2024-0043.
- 6. Kodi, R., Ravuri, M. R., Veeranna, V., Khan, M. I., Abdullaev, S., & Tamam, N. (2023). Hall current and thermal radiation effects of 3D rotating hybrid nanofluid reactive flow via stretched plate with internal heat absorption. Results in Physics, 53, Article 106915. https://doi.org/10.1016/j.rinp.2023.106915.
- 7. Raju, K. V., Mohanaramana, R., Reddy, S. S., & Kodi, R. (2023). Chemical radiation and Soret effects on unsteady MHD convective flow of Jeffrey nanofluid past an inclined semi-infinite vertical permeable moving plate. Communications in Mathematics and Applications, 14(1), 237–255.
- 8. Vaddemani, R. R., Ganta, S., & Kodi, R. (2023). Effects of Hall current, activation energy and diffusion thermo of MHD Darcy-Forchheimer Casson nanofluid flow in the presence of Brownian motion and thermophoresis. Journal of Advanced Research in Fluid Mechanics and Thermal Sciences, 105(2), 129-145. https://doi.org/10.37934/arfmts.105.2.129145
- 9. Kodi, R. (2023). Study of heat and mass transfer of an unsteady magnetohydrodynamic nanofluid flow past a vertical porous plate in the presence of chemical reaction, radiation and Soret effects. Journal of Nanofluids, 12, 767–776. https://doi.org/10.1166/jon.2023.1923.
- 10. Kodi, R., Ramana, R. M., Reddy, V. R., & Obulesu, M. (2023). Diffusion thermo and chemical reaction effects on magnetohydrodynamic Jeffrey nanofluid over an inclined vertical plate in the presence of radiation absorption and constant heat source. Journal of Nanofluids, 12, 147–156. https://doi.org/10.1166/jon.2023.1923
- 11. Shaw, S., Patra, A., Misra, A., Nayak, M. K., Chamkha, Ali J., (2021). A Numerical Approach to the Modeling of Thomson and Troian Slip on Nonlinear Radiative Microrotation of Casson Carreau Nanomaterials in Magnetohydrodynamics, Journal of Nanofluids, 10, 305-315, https://doi.org/10.1166/jon.2021.1790
- 12. Sastry, D.R.V.S.R.K., Kumar, N.N., Kameswaran, Kameswaran, P. K., Shaw, S., (2022). Unsteady 3D micropolar nanofluid flow through a squeezing channel: application to cardiovascular disorders, Indian Journal of Physics, 96, 57–70. https://doi.org/10.1007/s12648-020-01951-9
- 13. Nayak, M. K., Mahanta, G., Karmakar, K., Mohanty, P., Shaw S., (2022). Effects of thermal radiation and stability analysis on MHD stagnation casson fluid flow over the stretching surface with slip velocity, AIP Conference Proceedings, 2435, 020045. https://doi.org/10.1063/5.0084385.
- 14. Yadav, D., Awasthi, M. K., Ragoju, R., Bhattacharyya, K., Kodi, R., Hassan, M., & Wang, J. (2024). Impact of temperature-reliant thermal conductivity and viscosity variations on the convection of Jeffrey fluid in a rotating cellular porous layer. Proceedings of the Royal Society A: Mathematical, Physical and Engineering Sciences, 480(20240206). https://doi.org/10.1098/rspa.2024.0206.
- 15. Zhang, L., Vaddemani, R. R., Ganjikunta, A., Bingi, S., & Kodi, R. (2024). 3D-MHD mixed convection in a darcy-forchheimer maxwell fluid: Thermo diffusion, diffusion-thermo effects, and activation energy influence. Case Studies in Thermal Engineering, 61, Article 104916. https://doi.org/10.1016/j.csite.2024.104916.
- 16. Yadav, D., Awasthi, M. K., Ragoju, R., Bhattacharyya, K., Kodi, R., & Wang, J. (2024). The impact of rotation on the onset of cellular convective movement in a casson fluid saturated permeable layer with temperature-dependent thermal conductivity and viscosity deviations. Chinese Journal of Physics, 91, 262-277. https://doi.org/10.1016/j.ciph.2024.07.020.

- 17. Yedhiri, S. R., Palaparthi, K. K., Kodi, R., & Asmat, F. (2024). Unsteady MHD rotating mixed convective flow through an infinite vertical plate subject to Joule heating, thermal radiation, Hall current, radiation absorption. Journal of Thermal Analysis and Calorimetry. https://doi.org/10.1007/s10973-024-12954-7.
- 18. Kommaddi, H. B., Kodi, R., Ganteda, C., & Lorenzini, G. (2023). Heat and mass transfer on unsteady MHD chemically reacting rotating flow of Jeffrey fluid past an inclined plates under the impact of Hall current, diffusion thermo, and radiation absorption. Journal of Advanced Research in Fluid Mechanics and Thermal Sciences, 111(2), 225–241. https://doi.org/10.37934/arfmts.111.2.225241.
- 19. Kodi, R., Ali, F., Khalid, M., Abdullaeva, B. S., Altuijri, R., & Khan, M. I. (2023). Heat and mass transfer on MHD flow of Jeffrey nanofluid based on Cu and TiO₂ over an inclined plate and diffusion-thermo and radiation absorption effects. Pramana Journal of Physics, 97(202). https://doi.org/10.1007/s12043-023-02673-3.
- 20. Kodi, R., Vaddemani, R. R., Khan, M. I., Abdullaev, S. S., Habibullah, Boudjemline, A., Boujelbene, M., & Bouazzi, Y. (2023). Unsteady magneto-hydro-dynamics flow of Jeffrey fluid through porous media with thermal radiation, Hall current, and Soret effects. Journal of Magnetism and Magnetic Materials, 582, Article 171033. https://doi.org/10.1016/j.jmmm.2023.171033
- 21. Raghunath, K., Nagesh, G., Reddy, V. R., & Obulesu, M. (2021). Unsteady MHD fluid flow past an inclined vertical porous plate in the presence of chemical reaction with aligned magnetic field, radiation, and Soret effects. Heat Transfer, 51(6), 1-18. https://doi.org/10.1002/htj.22423
- 22. Reddy, V. R., Raghunath, K., & Obulesu, M. (2022). Characteristics of MHD Casson fluid flow past an inclined vertical porous plate. Materials Today: Proceedings, 49(5), 2136-2142. https://doi.org/10.1016/j.matpr.2021.08.328
- 23. Raghunath, K., Reddy, V. R., & Obulesu, M. (2021). Effects of radiation absorption and aligned magnetic field on MHD Casson fluid past an inclined vertical porous plate in porous media. In Simulation and Analysis of Mathematical Methods in Real-Time Engineering Applications (pp. 273–291). Wiley Scrivener Publishing LLC.
- 24. Kuznetsov, A. V., & Nield, D. A. (2010). Natural convective boundary-layer flow of a nanofluid past a vertical plate. International Journal of Thermal Sciences, 49, 243-247. http://dx.doi.org/10.1016/j.ijthermalsci.2009.07.015
- 25. Hamad, M. A. A., & Pop, I. (2011). Unsteady MHD free convection flow past a vertical permeable flat plate in a rotating frame of reference with constant heat source in a nanofluid. Heat and Mass Transfer, 47, 1517. http://dx.doi.org/10.1007/s00231-011-0816-6
- 26. Hamad, M. A. A., Pop, I., & Ismail, A. M. (2011). Magnetic field effects on free convection flow of a nanofluid past a vertical semi-infinite flat plate. Nonlinear Analysis: Real World Applications, 12, 1338-1346. http://dx.doi.org/10.1016/j.nonrwa.2010.09.014
- 27. Chamkha, A. J., & Aly, A. M. (2010). MHD free convection flow of a nanofluid past a vertical plate in the presence of heat generation or absorption effects. Chemical Engineering Communications, 198, 425-441. http://dx.doi.org/10.1080/00986445.2010.520232
- 28. Turkyilmazoglu, M., & Pop, I. (2013). Heat and mass transfer of unsteady natural convection flow of some nanofluids past a vertical infinite flat plate with radiation effect. International Journal of Heat and Mass Transfer, 59, 167-171. http://dx.doi.org/10.1016/j.ijheatmasstransfer.2012.12.009
- 29. Turkyilmazoglu, M. (2014). Unsteady convection flow of some nanofluids past a moving vertical flat plate with heat transfer. Journal of Heat Transfer, 136, 031704. http://dx.doi.org/10.1115/1.4025730
- 30. Kumar, B. R., Kumar, T. S., & Kumar, A. G. (2015). Thermal diffusion and radiation *Nanotechnology Perceptions Vol. 20 No.6 (2024)*

- effects on unsteady free convection flow in the presence of magnetic field fixed relative to the fluid or to the plate. Frontiers in Heat and Mass Transfer, 6. http://dx.doi.org/10.5098/hmt.6.12
- 31. Leong, K. Y., Ong, H. C., Gan, W. T., & Mahlia, T. M. I. (2018). Thermal conductivity of an ethylene glycol/water-based nanofluid with copper-titanium dioxide nanoparticles: An experimental approach. International Communications in Heat and Mass Transfer, 90, 23–28.
- 32. Ali, F., Aamina, I., Khan, N. A., Sheikh, M. G., & Tlili, I. (2018). Effects of different shaped nanoparticles on the performance of engine-oil and kerosene-oil: A generalized Brinkman-type fluid model with non-singular kernel. Scientific Reports, 8, 15285.
- 33. Vasheghani, M. H., Marzbanrad, E., Zamani, C., Aminy, M., & Raissi, B. (2013). Thermal conductivity and viscosity of TiO₂–engine oil nanofluids. International Journal of Nanomechanics Science and Technology, 4, 145–156.
- 34. Khata, N. D., Kadim, Z. K., & Khalaf, K. A. (2020). Numerical study of heat transfer enhancement in contour corrugated channel using water and engine oil. CFD Letters, 12, 17–23.
- 35. Raju, A., Ojjela, O., & Kambhatla, P. K. (2020). A comparative study of heat transfer analysis on ethylene glycol or engine oil as base fluid with gold nanoparticle in presence of thermal radiation. Journal of Thermal Analysis and Calorimetry, 145, 2647–2660.
- 36. Ravindranath Reddy, G., & Ramakrishna Reddy, G. (2022). Casson nanofluid performance on MHD convective flow past a semi-infinite inclined permeable moving plate in presence of heat and mass transfer. Heat Transfer, 1–21. https://doi.org/10.1002/htj.22645
- 37. Abbasi, F. M., Hayat, T., & Alsaadi, F. (2015). Peristaltic transport of magnetonanoparticles submerged in water: Model for drug delivery system. Physica E, 68, 123–132.
- 38. Abbasi, F. M., Hayat, T., & Alsaadi, F. (2015). Hydromagnetic peristaltic transport of water-based nanofluids with slip effects through an asymmetric channel. International Journal of Modern Physics B, 29, 1–17.
- 39. Ahmad, S., Ali, K., Nisar, K. S., et al. (2021). Features of Cu and TiO₂ in the flow of engine oil subject to thermal jump conditions. Scientific Reports, 11, 19592. https://doi.org/10.1038/s41598-021-99045-x
- 40. Cramer, K. P., & Pai, S. I. (1973). Magneto Fluid Dynamics for Engineers and Applied Physics. New York: McGraw-Hill Book Co.
- 41. Grief, G., Habib, I. S., & Lin, L. C. (1971). Laminar convection of a radiating gas in a vertical channel. Journal of Fluid Mechanics, 45, 513–520.